AIAA JOURNAL
Vol. 38, No. 8, August 2000

Technical Notes

TECHNICAL NOTES are short manuscripts describing new developments or important results of a preliminary nature. These Notes cannot exceed six manuscript pages and three figures; a page of text may be substituted for a figure and vice versa. After informal review by the editors, they may be published within a few months of the date of receipt. Style requirements are the same as for regular contributions (see inside back cover).

Numerical Investigation into Multiple Vortex Structures Formed over Flat End-Cap Wings

Deryl O. Snyder* and Robert E. Spall†
Utah State University, Logan, Utah 84322-4130

Nomenclature

c = wing chord
Re = Reynolds number based on wing chord, $U_\infty c/\nu$
S = scalar measure of the deformation rate tensor
S_{ij} = strain-rate tensor
U_∞ = freestream velocity
x = streamwise coordinate
y = spanwise coordinate
z = vertical coordinate
α = angle of attack
Ω_{ij} = rate-of-rotation tensor

Introduction

TIP vortices shed from finite-span wings are of considerable technological importance, with applications to airplane and submarine wings, helicopter rotor blades, and marine and aviation propellers, to name but a few. In nearly all instances, these vortices have undesirable effects, such as aerodynamic inefficiency, mechanical fatigue, and noise (cf. Ref. 1). Of primary interest in this investigation is the formation and very-near-field development of a tip vortex generated from a rectangular wing with a flat end-cap. This geometry is representative of that encountered in the deployment of flaps for high-lift configurations, where, for instance, tip vortex formation and near-field evolution is an important issue in noise control.

Previous experimental studies have shown that the vortex development process for flat end-caps is very different from that for rounded end-caps in that multiple shear-layer vortices exist in the vicinity of the wingtip.[2–5] Using hot-wire anemometry, Francis and Kennedy[2] observed, at a Reynolds number of 24.7×10^4 and an angle of attack of 4 deg, a single secondary vortex over the flat end-cap, which eventually merged with the primary suction-side vortex near the trailing edge. However, flow visualization studies by Shekarriz et al.[3,4] and Katz and Bueno Galdo[5] at lower Reynolds numbers ($3.7 \times 10^4 \leq Re \leq 2.2 \times 10^4$) and higher angles of attack ($\alpha \leq 12$ deg) showed multiple secondary vortices. These shear-layer vortices are not observed over rounded end-caps, since there is no tendency for the flow to separate as the fluid passes from the pressure side, across the cap, and to the suction side. Unfortunately, flow visualization of the secondary vortices is difficult because they originate within the wall boundary layer and can be quite small, making introduction of tracer fluid into the vortex problematic.

In addition to experimental work, Reynolds-averaged Navier–Stokes (RANS) calculations have also been performed previously to investigate the near-field structure of a wing-tip vortex. The vast majority of these studies has investigated wings with rounded or beveled end-cap geometries[6–10] and has shown that computational fluid dynamics (CFD) can accurately predict the initial roll-up stage. None of these studies, however, specifically investigated the development and merging process of multiple vortices that form over wings with flat end-caps. In a more recent work,[11] RANS calculations were performed for a generic high-lift configuration at flap deflections of 29 and 39 deg.

In the present work the formation and merging process of multiple vortex structures formed over flat end-caps is investigated through numerical solutions of the RANS equations. Both one-equation and differential Reynolds stress turbulence models have been employed.

Numerical Method and Turbulence Model

The steady, incompressible, RANS equations were integrated using an unstructured, segregated, pressure-based finite-volume procedure as implemented within the Fluent version 5.0 code (Fluent, Inc., Lebanon, New Hampshire). The RANS equations are well known and, hence, for purposes of brevity, are not shown (cf. Ref. 12).

In terms of the solution/discretization procedure, pressure–velocity coupling was achieved using the SIMPLEC (Ref. 13) algorithm. Differencing of the convective terms was implemented using a third-order, bounded QUICK (Ref. 14) interpolation scheme for the momentum equations and a second-order, bounded upwind scheme for all turbulence equations. The viscous terms were discretized using second-order central differencing. Pressures were interpolated to the cell faces using a second-order interpolation scheme.[15] Two turbulence models were used: a one-equation Spalart–Allmaras (S-A) model[16] and a differential Reynolds stress model (RSM).[17,18]

The S-A model employed was slightly modified from the form originally proposed in Ref. 16. The modification combines measures of both rotation and strain tensors in the definition of the scalar measure of the deformation tensor (S) as[6]

$$S = (|\Omega_{ij}| + C_{\text{prod}} \min(0, |S_{ij}| - |\Omega_{ij}|)) \tag{1}$$

where $|\Omega_{ij}| = \sqrt{(2\Omega_{ij}\Omega_{ij})}$, $|S_{ij}| = \sqrt{(2S_{ij}S_{ij})}$, and C_{prod} is a constant. The case of $C_{\text{prod}} = 0.0$ corresponds to the original form of the model. The justification for originally neglecting the mean strain was that, for wall-bounded flows (which were of primary interest in the development of this model), turbulence is found primarily where vorticity is generated near walls. However, by including the mean strain in this fashion, the production of eddy viscosity is reduced in regions where the vorticity exceeds the strain rate. This feature is desirable for vortical flows, where the damping effects of solid-body rotation diminish turbulence production near the vortex core. Based on the work presented in Ref. 6 for flow over wings with round end-caps, a value of $C_{\text{prod}} = 2.0$ was employed.

Solutions were also calculated using a differential RSM. Here, transport equations for the Reynolds stresses as well as for the dissipation rate are solved, leading to seven additional transport equations. The RSM inherently accounts for the effects of streamline curvature, swirl, and rapid changes in strain rate but is substantially more computationally expensive than one- and two-equation models. The accuracy of RSM solutions is strongly dependent upon the closure assumptions for the dissipation-rate and pressure–strain terms of the Reynolds stress transport equation. We present results obtained using the quadratic pressure–strain model of Speziale et al.,[19] which has been shown to provide improved performance over linear models, particularly in flows with streamline curvature. However, additional calculations using a linear model, which for

Received 13 September 1999; revision received 29 December 1999; accepted for publication 5 January 2000.

*Graduate Student. Student Member AIAA .
†Associate Professor. Senior Member AIAA.

purposes of brevity are not presented, revealed no discernible difference in the vortex structure. The dissipation term was modeled by an isotropic dissipation rate. The turbulent diffusive transport term was modeled using a simplified form of the generalized gradient diffusion model of Daly and Harlow,[20] employing a scalar turbulent diffusivity.[21] Nonequilibrium wall functions were used to implement the wall boundary conditions.

Computational Grid

Although the flow solver utilized unstructured grids, a multiblock, structured grid was first developed for use in this work. Multiblock structured grids have considerable potential to achieve favorable grid smoothness and orthogonality, while retaining flexibility in the gridding of complex geometries. However, generating quality grids through the use of a large number of blocks is often the most time-consuming aspect of the CFD process. To address this issue, Eiseman[22] has developed a technique that automates much of the structured grid generation process. This methodology, which is available commercially in the form of the GridPro/az3000 grid generation package used in this work, relies primarily on the user to input the appropriate wire-frame grid topology that need only roughly follow bounding surfaces. Other factors, such as surface grid generation and zone construction, are handled as part of the grid generation solution process. This procedure allows one quickly to develop quite complex multiblock grid topologies with a minimum level of user intervention. This grid was then converted to an unstructured format for import into the solver.

A perspective view of the computational geometry employed in this study is shown in Fig. 1a. The wing modeled a rectangular, symmetric NACA 0015 airfoil, with a semispan aspect ratio of 2.0. Consistent with previous experimental studies, the wing was confined within tunnel walls. However, to ease computational requirements, the wall boundary layers were not modeled; rather, slip wall conditions were imposed. The computational domain was bounded by $-3c \le x \le 7c$, $-2c \le y \le 2c$, and $-22c \le z \le 2c$, with the origin located at the leading edge of the wing tip. At the inlet, fixed velocity and turbulence parameters were prescribed (turbulence intensity $=0.2\%$), whereas a zero-gradient condition was used at the outlet.

Two grids containing 15 blocks were generated: a coarse grid with approximately 820,000 cells and a fine grid with approximately 1.6 million cells. Figure 1b shows the grid structure near the wing tip for the coarse grid; the fine grid contained roughly double the cells in each direction in the tip region. Cells were heavily clustered around the tip as well as in the region of the trailing vortex for approximately one chord downstream. Normal spacing at the wing surface was $0.005c$. The unique grid structure on the flat end-cap, shown further in Fig. 1c, accurately conforms to the wing geometry, with no rounding of the sharp corners and no zero-volume cells or three-sided cell faces.

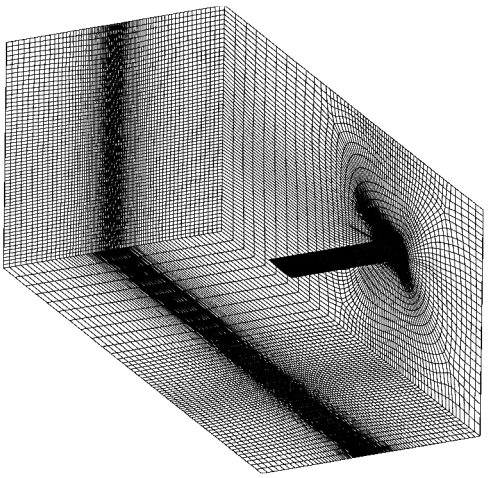

a) Perspective view of the computational domain

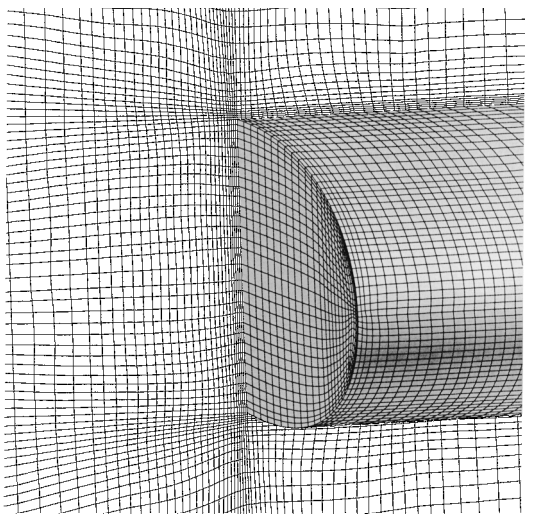

b) Grid structure in the wing-tip region

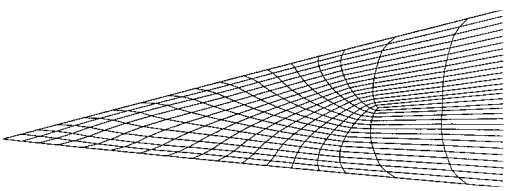

c) Grid structure near the trailing edge of the flat end-cap

Fig. 1 Computational mesh (coarse grid).

Results

The calculations were performed at a Reynolds number of 80×10^4 at angles of attack of 4 and 8 deg. Unless stated otherwise, the numerical results shown represent the fine-grid (1.6-million-cell) calculations. Results from the fine- and coarse-grid calculations were in excellent agreement (as shown in a subsequent figure); hence for the purposes and intent of this work, the solutions were deemed sufficiently grid converged.

The tip vortex structures observed in this study are shown in Fig. 2. Figure 2a shows planar velocity vectors at a chordwise location of $x/c = 0.75$ for the 4-deg-angle-of-attack case, while Fig. 2b displays the corresponding results at an 8 deg angle of attack, each computed using the S-A turbulence model. The results show that the flow is dominated by a primary suction-side vortex but contains one secondary shear-layer vortex located on the end-cap at $\alpha = 4$ deg (labeled S1 in Fig. 2a). At $\alpha = 8$ deg, multiple secondary vortices exist (labeled S1, S2, and S3 in Fig 2b). This observation is consistent with previous experimental results.[2–5] In the case of $\alpha = 8$ deg, the vortex labeled S3 rotates opposite the primary (P) and other two secondary vortices, S1 and S2. The formation of this vortex is due to interactions between the adjacent secondary vortices and the wing surface, rather than separation across the sharp corner. Results obtained using the RSM are presented in Figs. 2c and 2d. Consistent with the S-A solutions, single ($\alpha = 4$ deg) or multiple ($\alpha = 8$ deg) secondary vortices were predicted. Qualitative agreement between the models was also obtained in terms of vortex size and location. However, the diameters of vortices S2 and S3 as predicted using the S-A model are larger than those predicted using the RSM. In addition, the location of vortex S1 as predicted using the S-A model appears to be shifted slightly upward relative to the RSM prediction.

The streamwise development of the tip vortices is shown in Figs. 3a and 3b, which show contours of constant streamwise vorticity at several x/c locations for the $\alpha = 4$ and 8 deg calculations, respectively, as predicted by the S-A model. As observed in Ref. 2, a shear-layer vortex (S1 in Figs. 2a and 2b) begins to develop adjacent the suction side very near the leading edge, before development of the primary suction side vortex has begun. This vortex grows in strength as it progresses downstream and eventually merges with the primary vortex near the trailing edge. In addition, at $x/c = 0.1$, a small, counter-rotating vortex is seen near the suction side of the wing. This vortex, which is formed due to separation across the sharp corner, is quickly merged into the suction side vortex and its

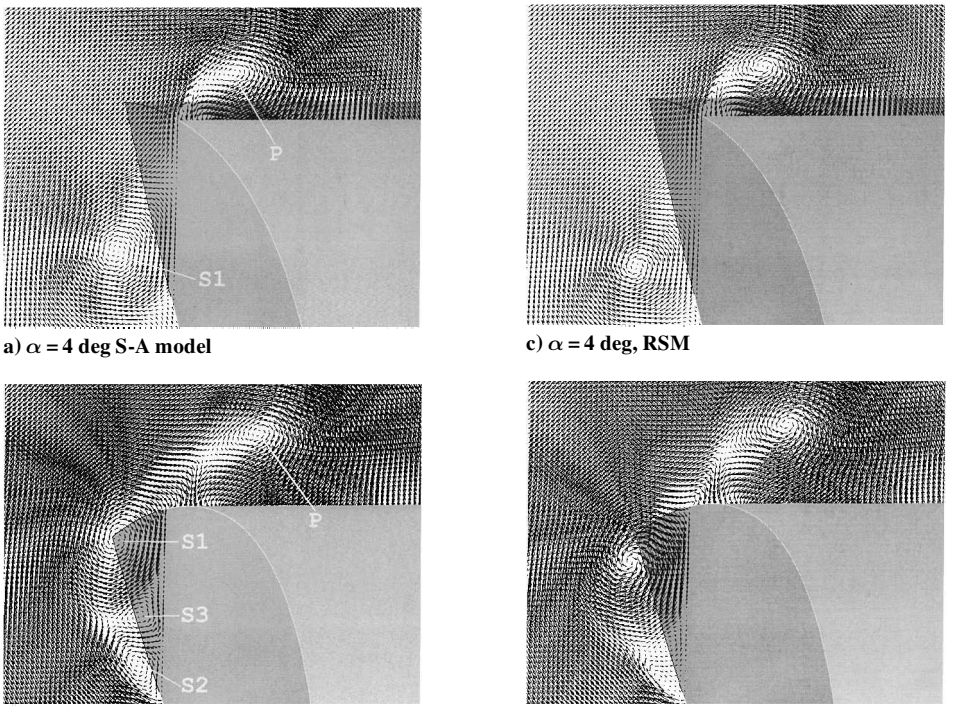

a) $\alpha = 4$ deg S-A model

c) $\alpha = 4$ deg, RSM

b) $\alpha = 8$ deg, S-A model

d) $\alpha = 8$ deg, RSM

Fig. 2 Velocity vectors at $x/c = 0.75$ and $Re = 80 \times 10^4$ showing the tip vortex structure.

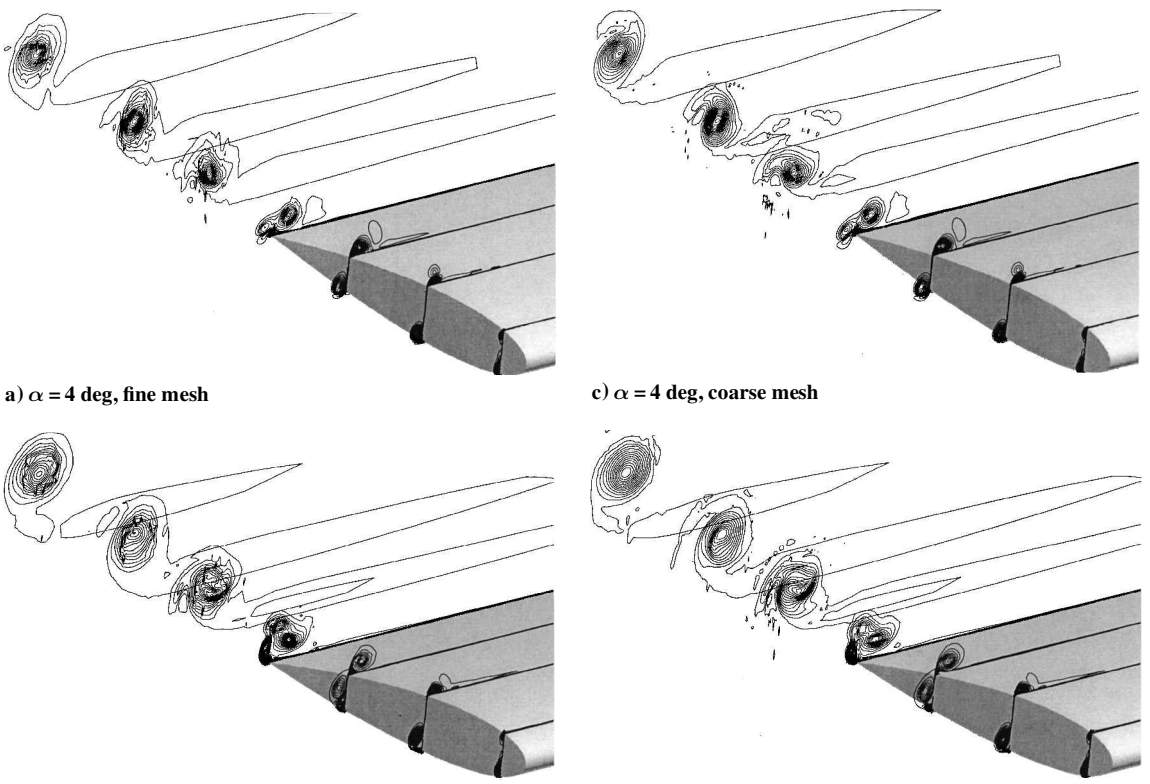

a) $\alpha = 4$ deg, fine mesh

c) $\alpha = 4$ deg, coarse mesh

b) $\alpha = 8$ deg, fine mesh

d) $\alpha = 8$ deg, coarse mesh

Fig. 3 Contours of constant axial vorticity at $x/c = 0.1$, 0.4, 0.7, 1.0, 1.3, 1.6, and 2.0 for $Re = 80 \times 10^4$ computed using the S-A model.

effects have all but disappeared by $x/c = 0.5$. (Hence it does not appear as a distinct vortex in Fig. 2.) The downstream stations in Fig. 3 reveal the rapidity of the roll-up process. The multiple vortices, which are quite distinct at $x/c = 1.0$, are essentially merged one chord downstream ($x/c = 2.0$). We also note an increase in the vortex core radii from $0.045c$ to $0.057c$ as α is increased from 4 to 8 deg. We also include in Figs. 3c and 3d solutions from calculations performed on the coarser (820,000-cell) grid. These results indicate that the solutions are sufficiently grid converged, particularly in the region of the wing end-cap, which is the primary area of interest.

Conclusions

Previous experimental studies have indicated that the tip vortex structure formed over wings with flat end-caps results from the merging of a primary suction-side vortex with one or more shear-layer vortices that develop over the end-cap. In the present study, both the S-A model and the differential RSM have been employed in calculating the flow over a NACA 0015 wing with a flat end-cap. The calculations revealed that at lower angles of attack ($\alpha = 4$ deg) one secondary vortex was formed, while at higher angles of attack ($\alpha = 8$ deg) three secondary vortices resulted, with the center vortex

rotating in the opposite direction from its neighbors. The qualitative flow patterns obtained were independent of the turbulence model used, although as one might expect, quantitative differences did exist between the S-A model and the RSM results. Although the present study was limited to a NACA 0015 plan form, it appears likely that, in general, these multiple vortex structures can be expected to form over most flat end-cap wings oriented at moderate angles of attack.

Acknowledgment

One of us (R.E.S.) would like to acknowledge partial support from NASA Langley Research Center under Grant NAG-1-1871.

References

[1]Green, S. I., "Wing Tip Vortices," *Fluid Vortices*, edited by S. I. Green, Kluwer Academic, Dordrecht, The Netherlands, 1995, pp. 427–470.

[2]Francis, M. S., and Kennedy, D. A., "Formation of a Trailing Vortex," *Journal of Aircraft*, Vol. 16, No. 3, 1979, pp. 148–154.

[3]Shekarriz, A., Fu, T. C., Katz, J., Liu, H. L., and Huang, T. T., "Study of Junction and Tip Vortices Using Particle Displacement Velocimetry," *AIAA Journal*, Vol. 30, No. 1, 1992, pp. 145–152.

[4]Shekarriz, A., Fu, T. C., Katz, J., and Huang, T. T., "Near-Field Behavior of a Tip Vortex," *AIAA Journal*, Vol. 31, No. 1, 1993, pp. 112–118.

[5]Katz, J., and Bueno Galdo, J., "Effect of Roughness on Rollup of Tip Vortices on a Rectangular Hydrofoil," *Journal of Aircraft*, Vol. 26, No. 3, 1989, pp. 247–253.

[6]Dacles-Mariani, J., Zilliac, G. G., Chow, J. S., and Bradshaw, P., "Numerical/Experimental Study of a Wingtip Vortex in the Near Field," *AIAA Journal*, Vol. 33, No. 9, 1995, pp. 1561–1568.

[7]Dacles-Mariani, J., Kwak, D., and Zilliac, G., "Incompressible Navier–Stokes Simulation Procedure for a Wingtip Vortex Flow Analysis," *Proceedings of the 6th International Symposium on Computational Fluid Dynamics*, Lake Tahoe, NV, 1995, pp. 224–230.

[8]Hsiao, C.-T., and Pauley, L. L., "Numerical Study of the Steady-State Tip Vortex Flow Over a Finite-Span Hydrofoil," *Journal of Fluids Engineering*, Vol. 120, 1998, pp. 345–353.

[9]Srinivasan, G. R., and McCroskey, W. J., "Navier–Stokes Calculations of Hovering Rotor Flowfields," *Journal of Aircraft*, Vol. 25, No. 10, 1988, pp. 865–874.

[10]Srinivasan, G. R., Baeder, J. D., Obayashi, S., and McCroskey, W. J., "Flowfield of a Lifting Rotor in Hover: A Navier–Stokes Simulation," *AIAA Journal*, Vol. 30, No. 10, 1992, pp. 2371–2378.

[11]Khorrami, M. R., Singer, B. A., and Radeztsky, R. H., "Reynolds-Averaged Navier–Stokes Computations of a Flap-Side-Edge Flowfield," *AIAA Journal*, Vol. 37, No. 1, 1999, pp. 14–22.

[12]Hinze, J. O., *Turbulence*, McGraw–Hill, New York, 1975.

[13]Vandoormaal, J. P., and Raithby, G. D, "Enhancements of the SIMPLE Method for Predicting Incompressible Fluid Flows," *Numerical Heat Transfer*, Vol. 7, 1984, pp. 147–163.

[14]Leonard, B. P., and Mokhtari, S., "ULTRA-SHARP Nonoscillatory Convection Schemes for High-Speed Steady Multidimensional Flow," NASA TM 1-2568 (ICOMP-90-12), 1990.

[15]Barth, T. J., and Jespersen, D., "The Design and Application of Upwind Schemes on Unstructured Meshes," AIAA Paper 89-0366, 1989.

[16]Spalart, P., and Allmaras, S., "A One-Equation Turbulence Model for Aerodynamic Flows," AIAA Paper 92-0439, 1992.

[17]Launder, B. E., Reece, G. J., and Rodi, W., "Progress in the Development of a Reynolds-Stress Turbulence Closure," *Journal of Fluid Mechanics*, Vol. 68, pp. 537–566.

[18]Gibson, M. M., and Launder, B. E., "Ground Effects on Pressure Fluctuations in the Atmospheric Boundary Layer," *Journal of Fluid Mechanics*, Vol. 86, 1978, pp. 491–511.

[19]Speziale, C. G., Sarkar, S., and Gatski, T. B., "Modelling the Pressure-Strain Correlation of Turbulence: An Invariant Dynamical Systems Approach," *Journal of Fluid Mechanics*, Vol. 227, 1991, pp. 245–272.

[20]Daly, B. J., and Harlow, F. H., "Transport Equations in Turbulence," *Physics of Fluids*, Vol. 13, 1970, pp. 2634–2649.

[21]Lien, F. S., and Leschziner, M. A., "Assessment of Turbulent Transport Models Including Non-Linear RNG Eddy-Viscosity Formulation and Second-Moment Closure," *Computers and Fluids*, Vol. 23, No. 8, 1994, pp. 983–1004.

[22]Eiseman, P. R., "Automatic Structured Grid Generation," *Computational Fluids Dynamics Review*, edited by M. Havez and K. Oshima, Wiley, Chichester, England, U.K., 1995.

R. M. C. So
Associate Editor

Predictor–Corrector Approach for the Analysis of Sandwich Panels

Jin Woo Park* and Yong Hyup Kim†
Seoul National University, Seoul 151-742, Republic of Korea

I. Introduction

THE through-the-thickness distribution of displacements and stresses of sandwich panels can be evaluated with multiple three-dimensional finite elements in the thickness direction[1,2] or with two-dimensional finite element models that allow higher-order shear deformations.[3] However, these approaches require substantial computational cost. More cost-effective approaches for the evaluation of stresses include postprocessing-type procedures that utilize the three-dimensional stress-equilibrium equations combined with finite element models based on the first-order shear-deformation theory.[4–6]

In this Note, through-the-thickness distributions of displacements as well as stresses of sandwich panels are evaluated by a postprocessing-type approach. A postprocessing predictor–corrector procedure has been utilized for the analysis of multilayered composite panels.[6] However, the procedure, if applied directly, yields inaccurate results for sandwich panels because of the large difference of material properties between the face sheets and the core. For the present study, the procedure is modified and applied to the analysis of sandwich panels with multilayered composite face sheets. The sandwich panel is subjected to both mechanical and thermal loading.

The effectiveness of the present procedure is demonstrated by means of numerical examples of the sandwich panels composed of multilayered composite face sheets and core with various elastic moduli. The solutions obtained by the present procedures are compared with the exact solutions of the three-dimensional thermoelasticity equations of the panel.[7]

II. Finite Element Model

The finite element used in conjunction with the proposed procedure is an assumed strain solid element based on the Hellinger–Reissner variational principle.[8] The present finite element model uses two unknowns: assumed displacements and independently assumed strains. The assumed strains play the role of reducing the locking effects and suppressing the spurious kinematic modes. Each element has two nodes in the thickness direction, with nine nodes on each of the top and the bottom surfaces. Each node has only three translational degrees of freedom. Rotational degrees of freedom are represented by the differences of the translational degrees of freedom at the top and the bottom surfaces. A detailed description of the formulation can be found in Ref. 8.

III. Predictor–Corrector Procedures

In the predictor procedure, through-the-thickness distributions of the in-plane stresses are evaluated by the superconvergent recovery technique presented by Zienkiewicz and Zhu.[9] Based on the in-plane stresses and utilizing the stress-equilibrium equations, the evaluation of the transverse stresses is by piecewise integration in the thickness direction of the panel. The equations for the evaluation of transverse stresses can be represented as follows:

Received 14 October 1999; revision received 12 January 2000; accepted for publication 27 March 2000.

*Research Assistant, Department of Aerospace Engineering, College of Engineering, San 56-1, Shinrim-Dong, Kwanak-Ku; jwpark@aeroguy.snu.ac.kr.

†Associate Professor, Department of Aerospace Engineering, College of Engineering, San 56-1, Shinrim-Dong, Kwanak-Ku; yhkim@gong.snu.ac.kr. Member AIAA.